Complex kinetics of DNA condensation revealed through DNA twist tracing

Wei Li,[1,*] Wei Juan Wong,[2,3] Ci Ji Lim,[2,3] Hai-Peng Ju,[1] Ming Li,[1] Jie Yan,[2,3,†] and Peng-Ye Wang[1,‡]

[1]*Beijing National Laboratory for Condensed Matter Physics and Key Laboratory of Soft Matter Physics, Institute of Physics, Chinese Academy of Sciences, Beijing 100190, China*

[2]*Department of Physics, National University of Singapore, Singapore 117542*

[3]*Mechanobiology Institute, National University of Singapore, Singapore 117411*

(Received 1 March 2015; revised manuscript received 24 May 2015; published 13 August 2015)

Toroid formation is an important mechanism for DNA condensation in cells. The length change during DNA condensation was investigated in previous single-molecule experiments. However, DNA twist is key to understanding the topological kinetics of DNA condensation. In this study, DNA twist as well as DNA length was traced during the DNA condensation by the freely orbiting magnetic tweezers and the tilted magnetic tweezers combined with Brownian dynamics simulations. The experimental results disclose the complex relationship between DNA extension and backbone rotation. Brownian dynamics simulations show that the toroid formation follows a wiggling pathway which leads to the complex DNA backbone rotation as revealed in our experiments. These findings provide the complete description of multivalent cation-dependent DNA toroid formation under tension.

DOI: 10.1103/PhysRevE.92.022707 PACS number(s): 82.37.Rs, 82.39.Pj, 87.15.La

I. INTRODUCTION

In cells and viruses, various efficient mechanisms have been evolved to package genomic DNA into a compact organization. In cells, such packaging is mainly achieved by DNA architectural proteins such as histones in eukaryotic cells and nucleoid associated proteins in prokaryotic cells [1–3]. There are other important mechanisms such as protamine mediated DNA condensation in mammalian sperms and polyamines mediated DNA organization in double-stranded DNA viruses [4,5]. *In vivo*, cations modulate the electrostatics of nucleic acids and play a fundamental role in DNA topology. Electron microscopy (EM) and cryoelectron microscopy (cryo-EM) imaging experiments have suggested that polyamines and multivalent cations organize DNA into the regular toroids [6,7]. To elucidate the mechanism underlying DNA condensation at single-molecule level, magnetic tweezers (MT) and optical tweezers (OT) have been employed to investigate the condensation dynamics *in vitro* by tracing the change of DNA length [8–14].

Toroid has been considered as a canonical form of DNA condensation and previous theoretical modeling was based on the helical toroid assumption [15–17]. According to the White-Fuller theorem: $Lk = Wr + Tw$ [18,19] (Lk, Wr, and Tw are the linking number, writhe, and twist of DNA chain, respectively), each toroid formation (the change of writhe) will cause a corresponding DNA twist change for twist-constrained DNA. Recording DNA backbone rotation (DNA twist) as well as the length change will lead to a deeper understanding of DNA condensation. In this paper, the DNA condensation mechanism was revisited by a combination of single molecule experiments and Brownian dynamics simulations, where DNA length and DNA twist were traced simultaneously.

II. SINGLE MOLECULE MANIPULATION FOR DNA CONDENSATION

First, the length tracing during DNA condensation was performed in 1 mM cobalt hexamine (10 mM phosphate, pH 7.5) by conventional magnetic tweezers, where one 10 102 bp DNA labeled with single digoxigenin and biotin at two ends was anchored to an antidigoxigenin coated cover slip and a 1 μm superparamagnetic streptavidin coated Myone bead (Invitrogen), respectively [Fig. 1(a)]. The DNA tether was originally stretched under a large force ($\sim$10 pN) to avoid any possible looping before measurement. Then the tension was reduced to an intended value and DNA length was measured. The toroid formation, which is characterized by stepwise length decrease, is clearly shown in Fig. 1(b) at 1.2 ± 0.05 pN. These results are consistent with previous experiments [10–12]. More than 100 experiments were repeated under different tensions and the distribution of step size (P) with respect to tension (F) was calculated. As shown in the inset of Fig. 1(b), the relation of step size and tension is consistent with the toroid assumption: the most probable loop size P is determined by $P = 2\pi\sqrt{k_B T A/2F}$, where A is the persistence length of DNA and F is the tension [20].

To obtain the DNA twist dynamics in condensation, the freely orbiting magnetic tweezers originally proposed by Lipfert *et al.* were employed [21]. A cylindrical magnet above the DNA sample was precisely adjusted to ensure that the preferred magnetization axis of the bead was aligned in the z direction. In the geometry, the bead will freely rotate around the z axis while tracing out a circle and the twist change of the tether can be discerned in real time [Fig. 1(c)] (please find more details in Ref. [21]). In this work, 1 μm Myone bead was used to trace the DNA twist and the temporal resolution was enough for discriminating DNA condensation within ten minutes. Before the real measurement with freely orbiting magnetic tweezers, some tests were carried out for the DNA molecule with conventional magnetic tweezers. To check whether a single DNA molecule was bound to the bead and the cover slip surface, we rotated the magnets about 50 turns at $\sim$10 pN. If the bead was tethered by more than one DNA molecule,

*Corresponding author: weili007@iphy.ac.cn
†Corresponding author: phyyj@nus.edu.sg
‡Corresponding author: pywang@iphy.ac.cn

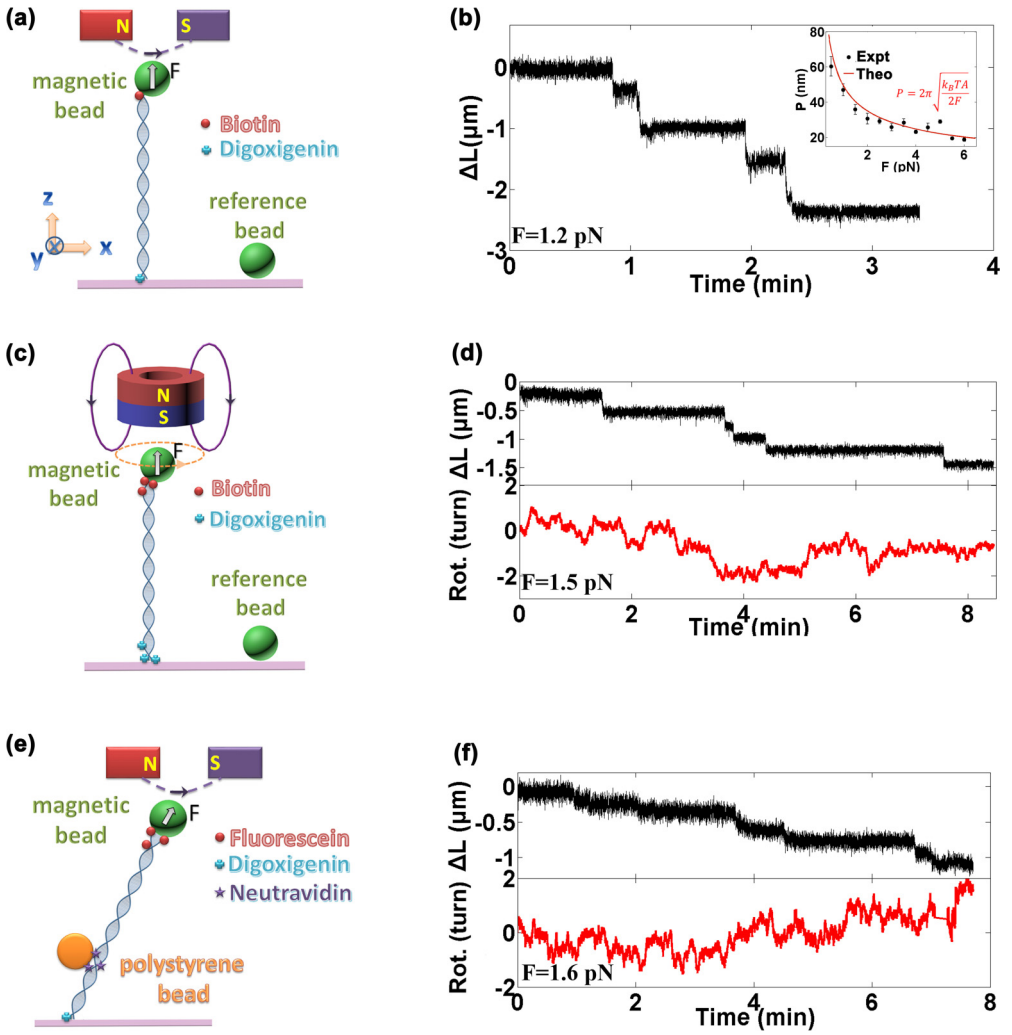

FIG. 1. (Color online) (a) With the conventional magnetic tweezers, DNA was anchored to a streptavidin-coated bead and a digoxigenin-coated cover slip. (b) The DNA length change was recorded in 1 mM cobalt hexamine and the relation between step size and tension is shown in the inset. (c) The torsion constrained DNA is trapped with freely orbiting magnetic tweezers. (d) The length and rotation were recorded simultaneously in DNA condensation under the same buffer conditions. (e) In the tilted magnetic tweezers, DNA was anchored to a streptavidin-coated bead and a digoxigenin-coated cover slip and an antifluorescein coated polystyrene was bound to DNA to trace the rotation of DNA backbone. (f) The extension and rotation were measured during DNA condensation with the tilted magnetic tweezers.

the bead would decrease to the surface dramatically. To check whether the DNA tether was not nicked, we rotated the magnets about 50 turns at ∼10 pN and reduced the tension gradually. If the extension began to decrease at about 2 pN as previous experiments [22], the plectonemic supercoils were formed and the DNA tether was not nicked. After these verifications, the magnets were changed to the cylindrical magnet for the real measurements. In 1 mM cobalt hexamine, DNA condensation was investigated at 1.5 ± 0.06 pN by tracing the DNA length and twist simultaneously [Fig. 1(d)]. In Fig. 1(d), the DNA length and corresponding DNA twist change are shown in the upper and the bottom panel, respectively. These results indicate that DNA extension abruptly decreases without apparent concurrent DNA twist change. At the end of DNA condensation, there is only a little DNA rotation decrease totally and no correlation between the length and twist change is found. We repeated the experiments and the similar results are revealed.

As an additional control experiment, we developed the tilted magnetic tweezers to record the DNA length and DNA twist simultaneously with two different beads. As shown in Fig. 1(e), one 15 658 bp DNA labeled with multifluorescein and single digoxigenin at two ends was anchored to a 1 μm superparamagnetic fluorescein coated carboxylic acid modified Myone bead (Invitrogen) and a antidigoxigenin coated cover slip, respectively. The streptavidin coated 1 μm polystyrene bead (ACME) was injected into the flow cell and incubated for about one hour to let the polystyrene bead bind to the multineutravidin labeled DNA fragment. In the conventional magnetic tweezers, the images of two beads were overlapped in CCD camera. To discriminate the two beads, the magnets were shifted in x direction to tilt the DNA tether with respect to z direction (Fig. 7). With the new tilted magnetic tweezers, the length of DNA chain can be traced by the superparamagnetic bead and the DNA backbone rotation traced by the polystyrene bead. Before the real measurement with tilted magnetic

tweezers, some tests were also carried out. To check whether a single DNA molecule was tethered, we rotated the magnets for about 50 turns in the conventional magnetic tweezers at about 10 pN, as we did in the previous experiment. To check whether the DNA tether was not nicked, we rotated the magnets at 0.5 turns/s for about 50 turns and recorded the polystyrene bead position. If the polystyrene bead rotated in the corresponding direction about 50 turns, the DNA tether was not nicked. After these verification, the magnets shifted in x direction and the measurement was carried out with the tilted magnetic tweezers. The measurement at 1.6 ± 0.08 pN shows that the DNA length is not always directly coupled to the DNA backbone rotation during DNA condensation [Fig. 1(f)], which is similar to the results revealed by freely orbiting magnetic tweezers. Why does DNA writhe change (DNA toroid formation) without a corresponding DNA twist change for a twist-constrained DNA as the White-Fuller theorem? To solve this puzzle, the dynamics of toroid formation during DNA condensation should be further investigated.

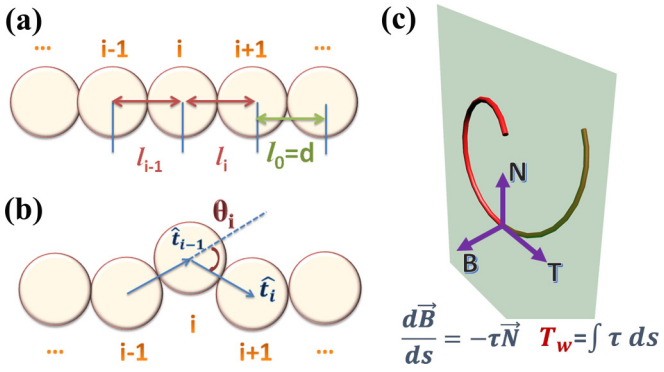

FIG. 2. (Color online) (a) Linear DNA molecule is modeled as a chain of 600 beads. The diameter d of each bead is 2 nm. (b) The ith bead connecting the $(i-1)$th and ith segments has bending angle θ_i. (c) In the Frenet-Serret frame, $\vec{T}$ is tangent vector, $\vec{N}$ normal vector, and $\vec{B}$ binormal vector.

III. BROWNIAN DYNAMICS WITH FRENET-SERRET MOVING FRAME

To bridge the gap between experimental and computational methods of studying dynamics of biological molecules, the coarse-grained molecular dynamics has been developed to investigate the dynamics of large biological molecules including DNA [23], RNA [24], and protein [25,26]. In the coarse-grained molecular dynamics, the degree number is reduced dramatically by clustering groups of atoms into new beads to reveal the dynamics of large biological molecules on a large time scale (up to microseconds). The simulation results can complement experiments to give detailed insight into the structure dynamics of these molecules, permitting us to understand the results of pervious DNA condensation experiments. Here, we performed the coarse-grained Brownian dynamics simulations to investigate the twist dynamics during DNA condensation.

In our simulation, DNA was modeled as a chain of 600 beads and the diameter d of each bead is set to 2 nm. The modeled DNA chain has a stretch modulus $\kappa = f_0/d$ with $f_0 = 1{,}500$ pN and a bending persistence length $A = 50$ nm according to the experimental values at physiological salt concentrations [27,28]. The total energy U of a given conformation includes the stretching energy U_{stretch} and the bending energy U_{bend}, which depends on the spatial positions of the beads $\vec{r}_i$ $(i = 1,2,\ldots)$. The force $\vec{f}_i$ is given by the negative gradient of the energy U: $\vec{f}_i = -\nabla_{\vec{r}_i} U$. In the overdamped limit, the trajectory of the ith bead in the time step Δt can be expressed by the following equation [29,30]:

$$\vec{r}_i(t+\Delta t) = \vec{r}_i(t) + (\vec{f}_i/\xi)\Delta t + \delta\vec{r}_i, \tag{1}$$

where $\xi = 3\pi\eta d$ is the translational drag coefficient and $\eta = 1.0$ cp is the viscosity of water at room temperature. $\delta\vec{r}_i$ is a random spatial displacement, following a Gaussian distribution with variance $\langle\delta\vec{r}_i\rangle^2 = 6D\Delta t$. Here, D is the translational diffusion coefficient which is related to the drag coefficient through the Einstein relation: $D = k_B T/\xi$. The time step $\Delta t = 0.1$ ns was chosen throughout the simulations. It is long enough to allow bead diffusion to occur and short enough to avoid overdisplacement during diffusion.

Because of high negative charge, DNA segments strongly repel each other. But if polyvalent cations are introduced into an aqueous solution, the interaction is mediated resulting in an attractive potential between DNA segments and DNA is observed to be condensed into toroid structure. To mimic the adhesion force during DNA condensation, a Morse potential was introduced between any two beads with an equilibrium distance at $l_0 = 2$ nm, $U_{i,j} = \varepsilon[e^{-2\alpha(d_{i,j}-l_0)} - 2e^{-\alpha(d_{i,j}-l_0)}]$, where $d_{i,j}$ is the center-to-center distance between ith bead and jth bead. The strength of interaction ε is set to $1.5k_BT$. α^{-1} defines a characteristic distance above which the interbead interaction is negligible (owing to electrostatic screening) and a fixed value $\alpha = 4$ nm^{-1} was chosen corresponding to a screening length 0.25 nm.

The theoretical Frenet-Serret moving frame has been widely applied to calculate DNA topology [31,32]. To obtain the twist involved in DNA condensation, the torque over the wrapped DNA chain in Frenet-Serret coordinates [33,34] is integrated. This integration defines a local Cartesian frame at any contour position s along a spatial curve $\vec{r}(s)$ by tangent vector $\hat{T} = \dot{\vec{r}}$, normal vector $\hat{N} = \frac{\dot{\hat{T}}}{|\dot{\hat{T}}|}$, and binormal vector $\hat{B} = \hat{T} \times \hat{N}$ [Fig. 2(c)]. Here $\cdot$ denotes the derivative $\frac{d}{ds}$. The twist of the frame along the curve is described by the Frenet-Serret formula: $\dot{\hat{T}} = \kappa'\hat{N}$, $\dot{\hat{N}} = -\kappa'\hat{T} + \tau_g\hat{B}$, and $\dot{\hat{B}} = -\tau_g\hat{N}$. Here $\kappa' = |\dot{\hat{T}}|$ is the curvature and $\tau_g = -\dot{\hat{B}}\cdot\hat{N}$ is the geometric torque. The twist in a DNA segment of $s_1 < s < s_2$ can be calculated from the torque by $\Phi_{s_1,s_2} = -\int_{s_1}^{s_2}\tau(s)ds$, and the total twist of the DNA is $\Phi_{0,L} = -\int_0^L \tau(s)ds$. In DNA chain, the Frenet-Serret frame $(\hat{T}_i, \hat{N}_i, \hat{B}_i)$ and its derivative $(\dot{\hat{T}}_i, \dot{\hat{N}}_i, \dot{\hat{B}}_i)$ were evaluated at each bead location.

The dynamics of the collapse of DNA chain into rodlike and toroid structures has been investigated with coarse-grained Brownian dynamics [35]. Here, to focus on the dynamics of toroid formation and to save computation time, we began the simulation with a preformed planar circular DNA loop with a diameter of 15 nm corresponding to the optimal DNA

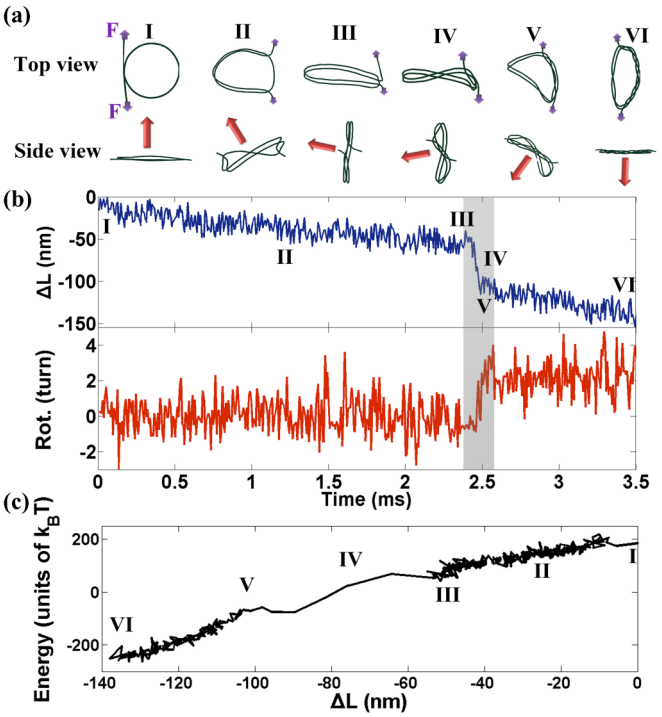

FIG. 3. (Color online) (a) Top and side view of snapshots of one round of the DNA wrapping process obtained from Brownian dynamics simulation. (b) DNA extension change and backbone rotation corresponding to the one-round of DNA wrapping. (c) Energy changes during the one round of DNA adsorption including DNA bending, stretching, and electrostatic interaction energies as well as the adsorption energy.

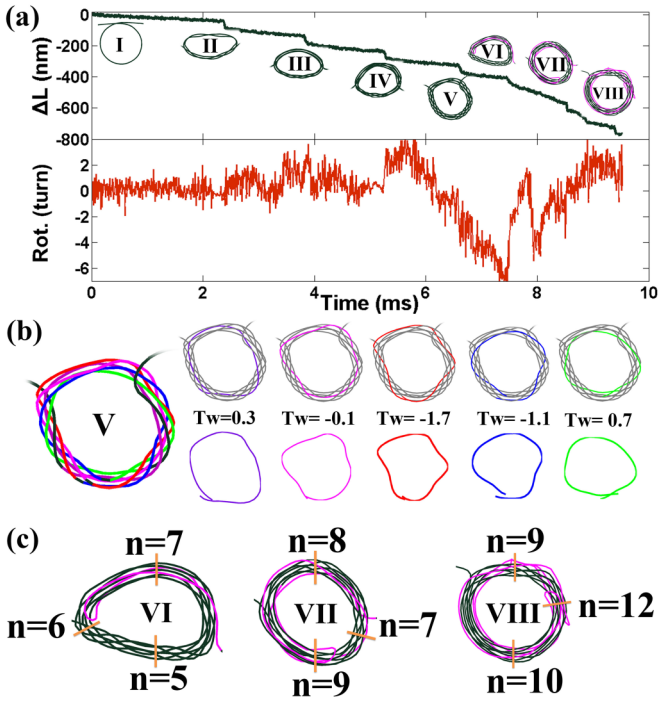

FIG. 4. (Color online) (a) DNA extension change and backbone rotation dynamics during a few rounds of DNA wrapping. (b) Each round of wrapping at stage V is differently colored to show the complex wiggling paths. (c) From stage VI to VIII, mixed forward and backward wrapping are shown.

looping size under 0.5 pN [20]. Figure 3(a) shows the top and side view of sequential snapshots during DNA condensation. During DNA absorption onto the loop, the initial DNA planar circular conformation is deformed. The loop uncovered by the second DNA becomes straightened and the whole loop adopts a bowlike conformation (II). During stage II, DNA is continuously adsorbed causing DNA extension reduction while not much DNA backbone rotation occurs, as revealed in Fig. 3(b) (bottom). When the first round of wrapping is completed (III and IV), the planar circular conformation is restored and is immediately followed by a spatial rotation of the planar circular conformation accompanied by absorption of additional DNA onto the toroid (V). It causes an abrupt, concurrent extension drop and DNA backbone rotation, as revealed by the shaded area in Fig. 3(b). Figure 3(c) shows the free energy landscape during this single round of wrapping.

In the process of condensation, a complex toroid is formed after several rounds of the DNA wrapping. Up to stage V [Fig. 4(a)], each DNA absorption stage is completed by a full round of DNA wrapping. For clarity, the DNA backbone is differently colored for each round of folding in the toroid at stage V [Fig. 4(b)], which reveals complex and irregular wiggling paths in these DNA loops. Such complex three-dimensional paths result in varying curvatures and torques. The values and signs of DNA twist change from one round of wrapping to another. Such negative and positive DNA backbone rotations contribute to a small net DNA backbone twist resulting from cancellations of the individual negative or positive DNA backbone rotations [Fig. 4(b)]. This explains why up to stage V, we do not observe significant DNA backbone rotations—wrapping of the first five rounds of DNA causes only −1.9 of net DNA backbone rotation [Fig. 4(a), bottom panel].

Besides the forward wrapping, there are also chances for nonabsorbed DNA interacting with the toroid behind the fork resulting in backward adsorption of DNA. In Fig. 4(a), such DNA folds caused by alternating forward and backward absorption are highlighted at stages VI–VIII. The mixed wrapping appears via a very common mechanism in the DNA wrapping process and leads to a complex relationship between DNA extension reduction and rotation. It also results in heterogeneous thickness of DNA at different regions on a toruslike condensate as illustrated in Fig. 4(c). Besides the most commonly observed toruslike wrapping, other conformations such as thick DNA bundles, the plectomeric supercoiled DNA structures, and their mixtures were also observed (Fig. 5), which indicates that the DNA condensation is a highly complex process.

IV. DISCUSSION AND CONCLUSION

Although a simple DNA model was used in our Brownian dynamics method, previous simulation combined with the Frenet-Serret calculation reveals the complex pathway of the toroid formation during DNA condensation and helps us understand the twist change as well as the length change in the process of DNA condensation. Here we compared the

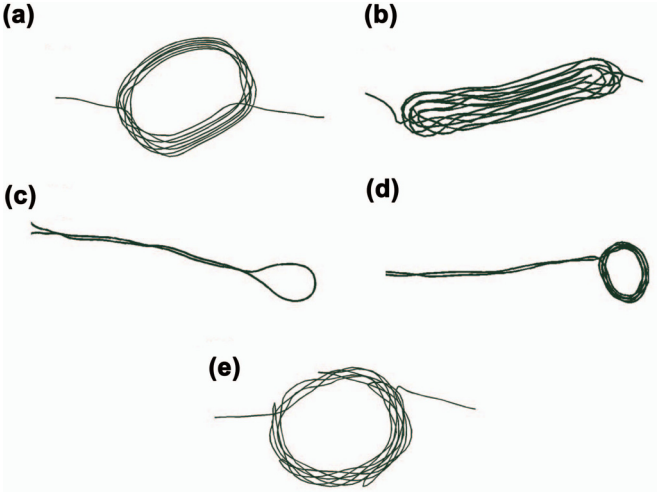

FIG. 5. (Color online) Results of Brownian simulation for DNA condensation under 0.5 pN. (a) Torus structure; (b) rodlike structure; (c) plectometic supercoiled DNA structure; (d) the hybrid of plectometic and torus structure; (e) the hybrid of torus and rodlike structure.

experimental results with the simulation results. As shown in Figs. 6(a) and 6(b), two typical types of DNA length and backbone rotation dynamics were recorded with the freely orbiting magnetic tweezers during DNA condensation at 1.0 pN, which includes extension decrease without concurrent DNA rotation (type I) and rotation without concurrent extension change (type II). In addition to the two types of condensation

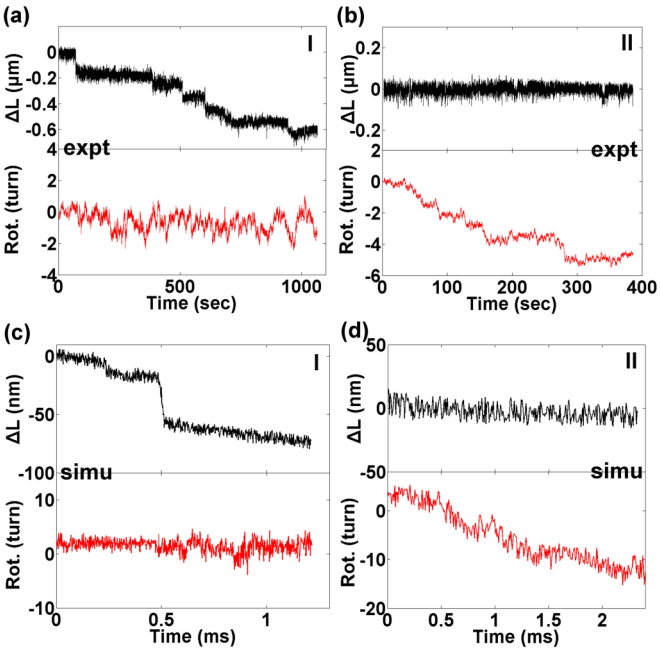

FIG. 6. (Color online) DNA condensation and rotational dynamics observed in experiments in 1.0 mM cobalt hexamine at a tension of 1.2 pN show extension decrease without concurrent DNA rotation [type I (a)] and apparent DNA rotation without DNA extension change [type II (b)]. Similar types of simulated time traces at a tension of 1.0 pN are shown in (c) and (d).

process, simulations also revealed other types such as stepwise folding with concurrent abrupt rotation, which often appeared during the few initial rounds of wrapping as shown in Figs. 3(a) and 3(b), but were rarely observed in our experiments. We speculate that this occurrence is associated with the ideal initial planar DNA loop used in simulations, whereas such an ideal initial conformation for DNA wrapping may not be present in the experiments. The different time scales of experiment and simulation are mainly due to the strong Morse potential chosen for the adhesion force between DNA segments. The adhesion force depends strongly on multivalent ion concentration [36]. In 1 mM cobalt hexamine, the critical adhesion force is about 3 pN. We carried our single molecule experiments in this relative weak ion concentration because small adhesion force will make the DNA condensation process slow and help us investigate the details of DNA condensation. In our simulations, the strength of interaction ε is set to $1.5k_BT$, which is much stronger than the experiment conditions. It is plausible to choose the strong adhesion interaction because the stable toroid is formed under these force field parameters. At the same time, DNA condensation will be finished in several microseconds under the strong adhesion interaction and it helps us save much computation time.

In summary, a highly complex picture of multivalent cation-induced DNA condensation is revealed by the combination of single molecule experiments (freely orbiting magnetic tweezers and tilted magnetic tweezers) and Brownian dynamics simulations through DNA twist tracing. The results suggest that DNA can be organized into highly diverse conformational states with different stabilities. These topologically distinct condensates result in complex DNA length change and backbone rotation dynamics. Frequently observed DNA rotation without apparent DNA extension change suggests that typically DNA folding occurs in two steps: an initial quick absorption of free DNA into condensates, possibly increasing its torsion energy, and a subsequent slower relaxation process to release the accumulated torsion energy. In the latter step, one would expect to observe DNA rotation without a significant change in DNA extension. An interesting observation is that DNA rotation observed in experiments consisted predominantly of DNA unwinding. Although the cause of the preferential DNA unwinding during DNA condensation is unclear, we speculate that it is associated with the chirality of the right-handed double helix structure of DNA. The findings provide the most complete description of multivalent cation-dependent DNA condensation under tension to date.

V. MATERIALS AND METHODS

A. DNA constructions

Preparation of torsion unconstrained DNA. The torsion-unconstrained DNA tether for conventional magnetic tweezers measurement is a PCR product. PCR amplification of lambda DNA was performed with the primers biotin-5 TATCTAGAGTATTGCCGTTGCTGTCTTTG and digoxigenin-5 CCGCCGGCACATAACAATCCTCGCACTCG. The product of 10 102 bp DNA were purified by QIAquick PCR Purification Kit (QIAGEN, Germany). The DNA was then diluted to 50 pM, aliquot and stored at $-80\,^{\circ}$C.

Preparation of torsion-constrained DNA. The torsion-constrained DNA tether for freely orbiting magnetic tweezers measurement contains three parts: an ∼1000 bp handle with multibiotin modification, ∼10000 bp central DNA, and an ∼1000 bp handle with multidigoxigenin modification. The total contour length of this tether is ∼3.5 μm. To prepare two handles, PCR amplification of lambda DNA was performed with the primers of 5′-TAGCCGGCGTATTGCCGTTGCTGTCTTTG, 5-GCCACC TCTTCCACCATCAGT and 5′-GCCACCTCTTCCACCAT CAGT, 5-TATCTAGAGTATTGCCGTTGCTGTCTTTG. To obtain multilabeled PCR products, Biotin-16-dUTP (Roche) and Digoxigenin-11-dUTP (Roche) were mixed. Then both products were purified by QIAquick PCR Purification Kit (QIAGEN, Germany) and digested overnight with NgoMIV and XbaI, respectively. The digested products were further purified with a QIAquick PCR Purification Kit, and their concentrations were determined by UV spectrometry. To produce the central DNA fragment for ligation, PCR amplification of lambda DNA was performed with the primers of biotin-5 TATCTAGAGTATTGCCGTTGCTGT CTTTG and digoxigenin-5-CCGCCGGCACATAACAA TCCTCGCACTCG. The product of 10 102 bp DNA was purified with a QIAquick PCR Purification Kit. The PCR product was digested by NgoMIV and XbaI. The digested products were purified with a QIAquick PCR Purification Kit. The two handles and central DNA fragment were ligated with T4 ligase at 16 °C overnight. An agarose gel was run to check the final product. Then, DNA was diluted to 50 pM, aliquot and stored at −20 °C.

Preparation of DNA samples for tilted magnetic tweezers. The DNA sample includes four parts: (1) an ∼1000 bp handle with multifluorescein modification, (2) ∼10000 bp central DNA, (3) an ∼1000 bp DNA fragment with multi-Neutravidin modification, and (4) an ∼3000 bp DNA handle with single-digoxigenin modification. To prepare two DNA handles, PCR amplification of pBR322 DNA was performed with the primers of 5′-CCTGACGAGCATCACAAA, 5′-GGG GTACCGCCATACCAAACGACGAG, and 5′-CGGGATCC TGTCCAGGCAGGTAGATGA, 5Dig-CAGAAACGCTGGT GAAAGT. To obtain multilabeled PCR products, Fluorescein-12-dUTP were mixed. Then both products were purified by QIAquick PCR Purification Kit (QIAGEN, Germany) and digested overnight with KpnI and BamHI, respectively. The digested products were further purified with a QIAquick PCR Purification Kit, and their concentrations were determined by UV spectrometry. To prepare the 10000 bp central DNA, PCR anmplification of lambda DNA was performed with the primers of 5′-GGGGTACCAACAGAGGAGGAGAAGAGTG and 5′-CCC AAGCTTTACCGATACTGCTGACCC. The purified PCR products were digested with KpnI and HindIII. To prepare ∼1000 bp DNA fragment with multi-Neutravidin modification, PCR anmplification of pBR322 DNA was performed with the primers of 5′-CCCAAGCTTCCTGACG AGCATCACAAA and 5′-CGGGATCCGCCATACCAA ACGACGAG. To obtain multilabeled PCR products, Neutravidin-16-dUTP were mixed. The purified PCR products were digested with HindIII and BamHI. The two handles and two DNA fragments were ligated with T4 ligase at 16 °C overnight. An agarose gel was run to check the final product. Then, DNA was diluted to 50 pM, aliquot and stored at −20 °C.

B. Experiments of the conventional magnetic tweezers

In the conventional magnetic tweezers, the 10 102 bp DNA molecule was bound at one end to a glass cover slip via bonds between digoxigenin and antidigoxigenin and to a magnetic Dynabead (Invitrogen Norway) at the other end via biochemical reactions between biotin and streptavidin, as shown in Fig. 1(a). Two small NdFeB magnets were used to stretch the DNA molecule. The real-time bead position was observed with a microscope objective (Olympus, 100×, 1.2, oil immersion), and the sample image was projected onto a JAI Giga-Ethernet CCD camera. The algorithm for the tracking bead position demonstrated remarkable accuracy, with the measurement uncertainty being typically approximately 1 nm in the x, y, and z directions.

C. Experiments of the freely orbiting magnetic tweezers

The principle of magnetic tweezers and the protocol for building a freely orbiting magnetic tweezers followed the general procedure described previously [21]. Briefly, the 3.5 μm DNA tether with being multibiotin and multidigoxigenin labeled two handles anchored to functioned coverslip and 1 μm Dynabead, as shown in Fig. 1(c). A cylindrical magnet with a hole in the center was used to stretch the DNA tether. Before actual measurement, the magnet position was tuned in x-y plane to let the beads fluctuations to trace out a circular trajectory. For the measurement, the real-time rotation angle of DNA tether was calculated by conversion of the (x, y) position to polar (r, θ) coordinates.

D. Experiments of the tilted magnetic tweezers

To anchor a single DNA labeled with multifluorescein at one end to carboxylic acid modified Myone bead, we first coated the Myone bead with antifluorescein as follows (details found in Invitrogen product description). (1) Resuspend the Myone beads for 30 min and transfer 1 ml to a tube. (2) Place the tube in a magnet for 2 min and remove the supernatant. (3) Remove the tube from the magnet and add 1 ml 15mM MES buffer (0.32 g MES dissolve in 100 ml distilled water, pH 6.0), vortex for 10 s. (4) Place on a magnet for 2 min and remove the supernatant. (5) Repeat steps (3) and (4). (6) Resuspend the Myone beads in 100 μl 15 mM MES buffer. (7) Add 100 μl EDC (10 mg/ml) and incubated on a roller for 30 min at room temperature. (8) Place the tube on a magnet for 2 min and remove the supernatant. (9) Add 400 μg antifluorescein, diluted in 15 mM MES buffer to 200 μl. (10) Incubated on a roller overnight at room temperature. (11) Place the tube in a magnet for 2 min and remove the supernatant. (12) Remove the tube from the magnet and add 1 ml PBS with 0.1% Tween-20; place on a roller mixer for 10 min. (13) Place the tube on a magnet for 2 min and remove the supernatant. (14) Repeat steps (12) and (13). (15) Resuspend the Myone beads in 100 μl PBS with 0.1% Tween20 and 0.1% BSA.

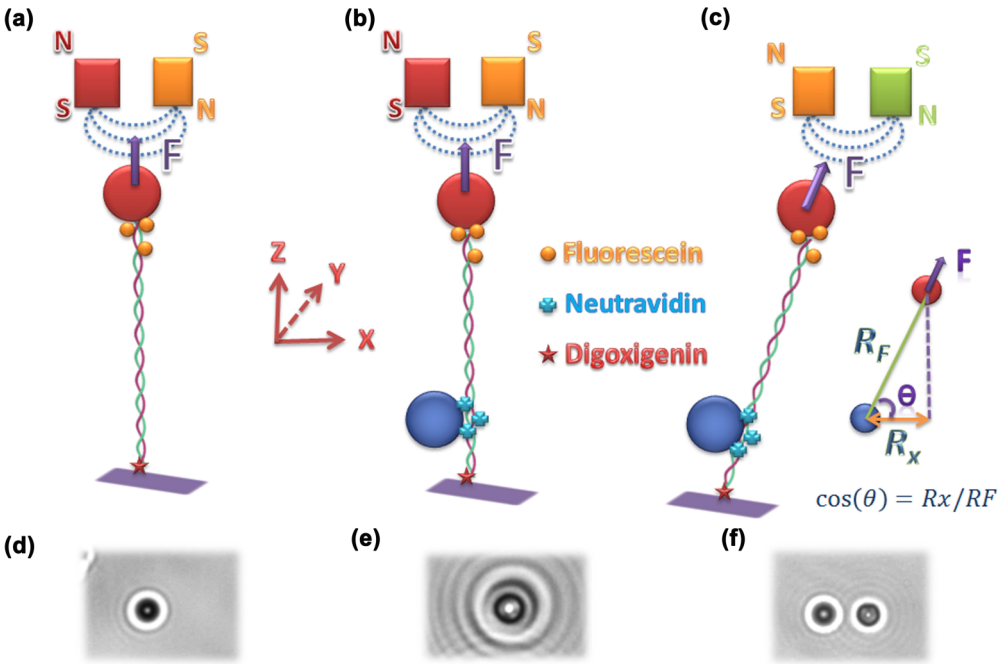

FIG. 7. (Color online) (a) and (d) Conventional magnetic tweezers and corresponding CCD image. (b) and (e) In conventional magnetic tweezers, the images of two beads bound on the new DNA sample are overlapped. (c) and (f) In tilted magnetic tweezers, the DNA is tilted and the images of the two beads were separated.

To trace the DNA length and rotation at the same time, we bind the two beads to the DNA sample as follows. (1) Add 10 μl antifluorescein coated Myone bead into 2 μl 50 pM DNA. (2) Place the tube on the roller mixture for about 30 min to bind the bead to DNA smaple. (3) Inject the DNA and Myone bead mixture into the flow cell and incubate for 1 h to anchor DNA sample to the surface of cover slip. (4) Rinse the flow cell with 500 μl PBS buffer (5 mg/ml BSA, PBS, pH 7.5). (5) Inject 50 μl streptavidin coated polystyrene bead (polystyrene in 0.25 mg/ml BSA, 0.3 percent Casein, PBS, pH 7.4) into the flow cell and incubate for 1 h to let the polystyrene bead bind to the DNA fragment labeled with Neutravidin. (6) Rise the flow cell with 500 μl PBS buffer (0.25 mg/ml BSA, 0.3% Casein, PBS, pH 7.4).

In the conventional magnetic tweezers, the two magnets were adjusted precisely and the DNA chain was stretched in z direction, as shown in Fig. 7(a). In this condition, the images of the magnetic bead and polystyrene bead were overlapped in CCD camera as shown in Figs. 7(b) and 7(e). To avoid the images of two beads being overlapped and to trace the positions of the two beads simultaneously, the magnets were shifted in x direction so that DNA chain were tilted with an angle θ to z direction, as shown in Figs. 7(c) and 7(f).

Because the DNA is tilted [Fig. 8(a)], the circle trajectory the polystyrene when DNA rotates is transformed to an ellipse trajectory [Fig. 8(b)]. Figure 8(c) is one trajectory of polystyrene in real measurements. We fit the trajectory with ellipse fitting algorithm to get best-fitting radius a and b of the corresponding trajectory and to rebuild the corresponding circle trajectory of the polystyrene [Fig. 8(d)]. The tilt angle θ can be derived by the relation $\sin(\theta) = a/b$.

In the measurement, we recorded the positions of the two beads in x-y plane: x_{mag}, y_{mag}, x_{poly}, and y_{poly}. The extension of DNA chain (ΔL) can be measured by $\Delta L = \sqrt{x_{\mathrm{mag}}^2 + y_{\mathrm{mag}}^2}/\cos(\theta)$ and the rotation can be measured by the conversion of the $(x_{\mathrm{poly}}, y_{\mathrm{poly}})$ position to polar (r, α) coordinates.

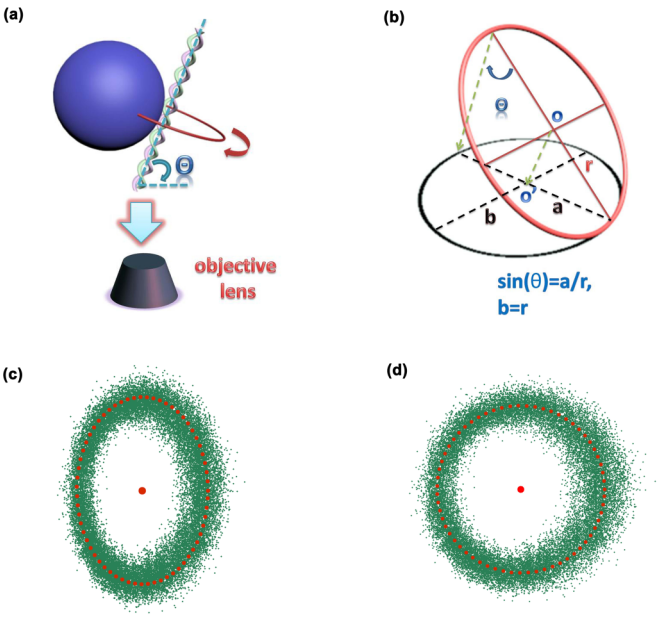

FIG. 8. (Color online) (a) Cartoon shows the tilted DNA image projects to CCD camera. (b) The circle trajectory is transformed to an ellipse trajectory with an angle θ. (c) The ellipse trajectory of polystyrene bead was recorded. (d) We fit the trajectory with an ellipse fitting algorithm to rebuild the circle trajectory.

ACKNOWLEDGMENTS

This research was supported by the National Nature Science Foundation of China (Grants No. 11104341, No. 11474346, No. 11274374, and No. 61275192), the 973 Program of China (Grant No. 2013CB837200), and the National Research Foundation of Singapore through the Mechanobiology Institute of Singapore.

W.L. and W.J.W. contributed equally to this work

[1] K. Luger, A. W. Mäder, R. K. Richmond, and D. F. Sargent, Nature (London) **389**, 251 (1997).
[2] A. Ishihama, Proc. Jpn. Acad. Ser. B Phys. Biol. Sci. **88**, 485 (2012).
[3] C. J. Lim, S. Y. Lee, J. Teramoto, A. Ishihama, and J. Yan, Nucl. Acids Res. **41**, 746 (2013).
[4] M. E. Wilson and L. K. Miller, Virology **151**, 315 (1986).
[5] Y. Liu, J. Wu, H. Chen, C. L. Hew, and J. Yan, Virology **408**, 197 (2010).
[6] V. A. Bloomfield, Biopolymers **31**, 1471 (1991).
[7] N. V. Hud and K. H. Dowing, Proc. Natl. Acad. Sci. USA **98**, 14925 (2001).
[8] C. G. Baumann, V. A. Bloomfield, S. B. Smith, C. Bustamante, M. D. Wang, and S. M. Block, Biophys. J. **78**, 1965 (2000).
[9] Y. Murayama, Y. Sakamaki, and M. Sano, Phys. Rev. Lett. **90**, 018102 (2003).
[10] K. Besteman, S. Hage, N. H. Dekker, and S. G. Lemay, Phys. Rev. Lett. **98**, 058103 (2007).
[11] B. van den Broek, M. C. Noom, J. van Mameren, C. Battel, F. C. MacKinstosh, and G. J. Wuite, Biophys. J. **98**, 1902 (2010).
[12] W. Li, P.-Y. Wang, J. Yan, and M. Li, Phys. Rev. Lett. **109**, 218102 (2012).
[13] Q. Shao, S. Goyal, L. Finzi, and D. Dunlap, Macromolecules **45**, 3188 (2012).
[14] A. Lee, A. Karcz, R. Akman, T. Zheng, S. Kwon, S.-T. Chou, S. Sucayan, L. J. Tricoli, J. M. Hustedt, Q. Leng, J. D. Kahn, A. J. Mixson, and J. Seog, Ang. Chem. Int. Ed. **53**, 10631 (2014).
[15] I. M. Kulić and H. Schiessel, Phys. Rev. Lett. **92**, 228101 (2004).
[16] C. Battle, B. van den Broek, and F. C. MacKintosh, Phys. Rev. E **80**, 031917 (2009).
[17] D. Argudo and P. K. Purohit, Biophys. J. **103**, 118 (2012).
[18] J. H. White, Am. J. Math **91**, 693 (1969).
[19] F. B. Fuller, Proc. Natl. Acad. Sci. USA **75**, 3557 (1978).
[20] T. Strick, J. Allemand, V. Croquette, and D. Bensimon, Prog. Biophys. Mol. Biol. **74**, 115 (2000).
[21] J. Lipfert, M. Wiggin, J. W. Kerssemakers, F. Pedaci, and N. H. Dekker, Nat. Commun. **2**, 439 (2011).
[22] B. Taneja, B. Schnurr, A. Slesarev, J. F. Marko, and A. Mondragon, Proc. Natl. Acad. Sci. USA **104**, 14670 (2007).
[23] T. E. Ouldridge, A. A. Louis, and J. P. K. Doye, Phys. Rev. Lett. **104**, 178101 (2010).
[24] L. Liu and S. J. Chen, PLos One **7**, e48460 (2012).
[25] Z. Zhang, K. Y. Sanbonmatsu, and G. A. Voth, J. Am. Chem. Soc. **133**, 16828 (2011).
[26] P. Setny and M. Zacharias, Nucl. Acids Res. **39**, 9118 (2011).
[27] M. D. Wang, H. Yin, R. Landick, J. Gelles, and S. M. Block, Biophys. J. **72**, 1335 (1997).
[28] C. Bustamante, J. F. Marko, E. D. Siggia, and S. Smith, Science **265**, 1599 (1994).
[29] R. L. Honeycutt, Phys. Rev. A **45**, 600 (1992).
[30] D. L. Ermak and J. A. McCammon, J. Chem. Phys. **69**, 1352 (1978).
[31] I. Tobias, D. Swigon, and B. D. Coleman, Phys. Rev. E **61**, 747 (2000).
[32] J. Bohr and K. W. Olsen, Phys. Rev. E **88**, 052714 (2013).
[33] B. R. Iyer and C. V. Vishveshwara, Phys. Rev. D **48**, 5706 (1993).
[34] G. H. M. Van der Heijden and J. M. T. Thompson, Nonlin. Dyn. **21**, 71 (2000).
[35] A. Montesi, M. Pasquali, and F. C. MacKintosh, Phys. Rev. E **69**, 021916 (2004).
[36] B. A. Todd, V. A. Parsegian, A. Shirahata, T. J. Thomas, and D. C. Rau, Biophys. J. **94**, 4775 (2008).